Coastal Dynamics 2017
Paper No. 140

NUMERICAL SIMULATION OF SEDIMENT TRANSPORT IN SURF AND SWASH ZONES USING OPENFOAM

Nikolaos Karagiannis[1], Theofanis Karambas[2] and Christopher Koutitas[3]

Abstract

A challenging approach regarding the modeling of sediment transport in surf and swash zones is hereby applied and tested against experimental data (Dette 1998). The combination of a hydrodynamic model developed on OpenFOAM platform and a morphodynamic one written in FORTRAN constitutes a holistic method for the simulation of the wave propagation and sediment transport caused by the hydrodynamic state which is formed by the interaction of the incident waves with the seabed. The above method is an iterative one, which means that the hydrodynamic OpenFOAM model is run first using the initial bed morphology and the results are used by the morphodynamic model which yields the new seabed under the formed hydrodynamic state. This procedure is repeated until convergence, namely the new seabed is practically the same with the previous one.

Key words: OpenFOAM, sediment transport, numerical modelling, surf and swash zones

1. Introduction

The surf and swash zones are of great research interest due to their contribution to the beach formation every season. Actually, they constitute the parts of the beach where sediment transport is taking place continuously following the hydrodynamic state that is created by the breaking waves in the surf zone and the respective overtopping in the swash zone. Erosion and deposition are the products of the turbulent and unsteady nature of the flow in these zones and their prediction constitutes a great challenge, even nowadays with many advanced numerical models at our disposal.

Furthermore, erosion can be devastating for coastal structures and adjacent properties as it can provoke their instability and consequently their failure which can end up to be devastating for human lives as well. Hence, specific measures must be taken in order to protect the coastal areas from the above occurrence which measures usually are soft or hard engineering solutions depending on the severity of each case. So, the numerical models constitute the tools to predict the behavior of the beach and provide suitable solutions to prevent the aforementioned devastating effects and shield the coastal zones.

The numerical approach which is presented in this work has initially launched by the authors (Karagiannis et al., 2016) to describe the scour in front of a vertical breakwater where the depth is considered practically constant and standing waves are formed in front of the structure. But the cases tested hereby are more challenging as the turbulent effects of the breaking waves are taken into consideration and the erosion/accretion in surf and swash zones are investigated.

Two models are combined in order to describe the bed formation under the load of the breaking waves on a beach slope. A hydrodynamic numerical model developed on OpenFOAM platform has been applied first to describe the hydrodynamic state which is formed by the incident waves and the respective results of this model are used as input data for the second morphodynamic model, written in FORTRAN, which yields the new seabed as it is formed under the imposed waves and hydrodynamic state. Then, the new seabed constitutes the input data for the first OpenFOAM model which yields the new hydrodynamic state under the interaction of the incident waves and the new seabed. This process is repeated until convergence, namely the new seabed which is arisen from the morphodynamic model is the practically same with the previous one.

The aforementioned former numerical model was created with the open source toolbox OpenFoam and the additional toolbox waves2Foam (Jacobsen et al., 2012). The RANS (Reynolds averaged Navier Stokes) equations have been solved simultaneously with the transport equations of the turbulence model k-ω SST,

which, after extended investigation, was found the most suitable for free surface cases, and the VOF (Volume of Fluid) method ones (Hirt and Nichols, 1981).
The second numerical model has been developed in FORTRAN, estimating the sheet flow sediment transport rates with the Camenen and Larson (2007) transport rate formula, as well as the bed load and suspended load over ripples (Karambas, 2012). Suspended sediment transport rate is incorporated by solving the depth-integrated transport equation for suspended sediment (Karambas, 2012). After that, the conservation equation of the sediment mass is applied for several time steps and the scour is computed.
The above iterative method is applied and compared satisfactorily with experimental data (Dette, 1998).

2. Governing Equations of the hydrodynamic model (OpenFOAM)

This section provides the governing equations of the hydrodynamic mathematical model, which is synthesized on the basis of OpenFOAM and solves the Navier – Stokes equations numerically using the Finite Volume Method. The InterFoam solver, which was created for multiphase flows, is available in OpenFoam libraries and used in this work as the most suitable for free surface problems. Free surface is tracked by the VOF method, while the k-ω SST turbulence model is used for the simulation of the turbulence effects.

2.1. *Continuity and RANS Equations*

The mathematical model solves the continuity equation, which is as follows :

$$\frac{\partial U_{\mathrm{i}}}{\partial \mathrm{x_i}} = 0 \tag{1}$$

in conjuction with the Reynolds Averaged Navier Stokes (RANS) equations, which are the following ones:

$$\frac{\partial(\rho \mathrm{U_i})}{\partial \mathrm{x_i}} + \rho U_{\mathrm{j}} \frac{\partial U_{\mathrm{i}}}{\partial \mathrm{x_j}} = -\frac{\partial \mathrm{p}}{\partial \mathrm{x_i}} + \rho \mathrm{g_i} + \frac{\partial}{\partial \mathrm{x_j}} \left[\mu \left(\frac{\partial U_{\mathrm{i}}}{\partial \mathrm{x_j}} + \frac{\partial U_{\mathrm{j}}}{\partial \mathrm{x_i}} \right) - \rho \overline{u_\iota{}' u_j{}'} \right] + \sigma_T \kappa_\gamma \frac{\partial \gamma}{\partial \mathrm{x_i}} \tag{2}$$

where U is the velocity, ρ is the density, g is the gravity acceleration, p is the pressure, μ is the dynamic viscosity, and $-\rho \overline{u_\iota{}' u_j{}'}$ is the Reynolds stress tensor which is equal to the following expression :

$$\tau_{ij} = -\rho \overline{u_\iota{}' u_j{}'} = \mu_t \left(\frac{\partial U_{\mathrm{i}}}{\partial \mathrm{x_j}} + \frac{\partial U_{\mathrm{j}}}{\partial \mathrm{x_i}} \right) - \frac{2}{3} \rho k \delta_{ij} \tag{3}$$

where μ_t is turbulent viscosity coefficient, k is the turbulence kinetic energy and δ_{ij} is the Kronecker delta. The last term in equation (2) represents the surface tension effect.

2.2. *Volume of Fluid Equation*

Volume of fluid method (Hirt and Nichols, 1981) is provided by OpenFOAM for the "tracking" of the free surface during free surface simulations. Using this method, every free surface computational cell is divided in two parts, one which represents the air volume and the other is equal to water volume. The calculation of the water-air portion in every cell is possible with the help of the scalar quantity γ, with its value fluctuating between 0 and 1. When the cell is full of water, γ is equal to 1 and when the cell is full of air, γ is equal to 0, while it takes intermediate value (between 0 and 1) when the cell contains both water and air. The γ value is calculated with the following equation for every free surface computational cell:

$$\frac{\partial \gamma}{\partial t} + \frac{\partial(\gamma \mathrm{U_i})}{\partial \mathrm{x_i}} + \frac{\partial[\gamma(1-\gamma)\mathrm{Ur_i}]}{\partial \mathrm{x_i}} = 0 \tag{4}$$

where U_r is a relative velocity.
Using γ, quantities like density or viscosity can be calculated for every free surface cell as follows:

$$\rho = \gamma \rho_{water} + (1-\gamma)\rho_{air} \tag{5}$$

$$\mu = \gamma \mu_{water} + (1-\gamma)\mu_{air} \tag{6}$$

2.3. *Turbulence Modelling*

The transport equations for the k-ω SST model are as follows (Menter F. R., 1993-1994):

$$\mu_t = \frac{\rho \alpha_1 k}{\max(\alpha_1 \omega, SF_2)} \tag{7}$$

$$\frac{\partial(\rho k)}{\partial t} + \frac{\partial(\rho k U_i)}{\partial x_i} = P_k - \beta^* \rho k \omega + \frac{\partial}{\partial x_i}\left[(\mu + \sigma_k \mu_t)\frac{\partial k}{\partial x_i}\right] \tag{8}$$

$$\frac{\partial(\rho \omega)}{\partial t} + \frac{\partial(\rho \omega U_i)}{\partial x_i} = \alpha S^2 - \beta \rho \omega^2 + \frac{\partial}{\partial x_j}\left[(\mu + \sigma_\omega \mu_t)\frac{\partial \omega}{\partial x_j}\right] + +2(1 - F_1)\rho\sigma_{\omega 2}\frac{1}{\omega}\frac{\partial k}{\partial x_i}\frac{\partial \omega}{\partial x_i} \tag{9}$$

where k is the turbulent kinetic energy and ω is the dissipation rate. The rest coefficients are given in literature.

2.4. *Wave generation and absorption*

Cnoidal waves are implemented at the left boundary of the model domain in order to investigate the model's hydrodynamic behaviour (comparing the results with Ting & Kirby's,1994 experimental ones), using the additional toolbox waves2Foam (Jacobsen et al. 2012). The equation implemented, describing the above waves at the inlet, is as follows:

$$\eta = \eta_2 + 6HCn^2(2K(m)\left(\frac{x}{L} - \frac{t}{T}\right), m) \tag{10}$$

where H is the wave height, L is the wavelength, T is the wave period and η_2 is the trough elevation. Further Cn is one of the Jacobi elliptic functions and K(m) is the complete elliptic integral of the first kind.

Moreover, sponge layers from waves2Foam libraries are implemented at the left and right end of the computational domain in order to avoid wave reflection which would affect the numerical results.
The wave attenuation at the sponge layers is described by the following equation:

$$a_R(\chi_R) = 1 - \frac{\exp(\chi_R^{3.5})ibed - 1}{\exp(1) - 1} \quad \gamma\iota\alpha\ \chi_R \in [0; 1] \tag{11}$$

where the α_R is used in the following equation :

$$\varphi = a_R \varphi_{computed} + (1 - a_R)\,\varphi_{target} \tag{12}$$

where φ may be the velocity or the quantity γ from the VOF equation.

3. Governing Equations of the morphodynamic model (FORTRAN)

The mode of sediment movement on the coast is usually divided into bed load, suspended load and sheet flow transport. Different model concepts are being presently used for the prediction of each one, which range from empirical transport formulas to more sophisticated bottom boundary layer models.

In the present work, the bed load transport (q_{sb}) is estimated with a quasi-steady, semi-empirical formulation, developed by Camenen, and Larson, (2007):

$$\Phi_b = \begin{cases} \frac{q_{sb,w}}{\sqrt{(s-1)g d_{50}^3}} = a_n \sqrt{\theta_{cw,net}}\,\theta_{cw,m} \exp(-b\frac{\theta_{cr}}{\theta_{cw}}) \\ \frac{q_{sb,n}}{\sqrt{(s-1)g d_{50}^3}} = a_n \sqrt{\theta_{cn}}\,\theta_{cw,m} \exp(-b\frac{\theta_{cr}}{\theta_{cw}}) \end{cases} \tag{13}$$

where the subscripts *w* and *n* correspond, respectively, to the wave direction and the direction normal to the wave direction, *s* (= ρ_s/ρ) is the relative density between sediment (ρ_s) and water (ρ), *g* the acceleration due to gravity, d_{50} the median grain size, a_w, a_n and *b* are empirical coefficients (Camenen and Larson 2007), $\theta_{cw,m}$ and θ_{cw} the mean and maximum Shields parameters due to wave-current interaction, θ_{cn} the current-related Shields parameter in the direction normal to the wave direction, and θ_{cr} the critical Shields parameter for the inception of transport. The net Shields parameter $\theta_{cw,net}$ in eq. 5 is given by:

$$\theta_{cw,net} = (1 - a_{pl,b})\theta_{cw,on} - (1 + \alpha_{pl,b})\theta_{cw.off} \tag{14}$$

where $\theta_{cw,on}$ and $\theta_{cw,off}$ are the mean values of the instantaneous Shields parameter over the two half periods T_{wc} and T_{wt} ($T_w = T_{wc} + T_{wt}$, in which T_w is the wave period and $\alpha_{pl,b}$ a coefficient for the phase-lag effects (Camenen and Larson 2007). The Shields parameter is defined by:

$$\theta_{cw,j} = \frac{1}{2} f_{cw} U_{cw,j}^2 / [(s-1) g d_{50}] \tag{15}$$

with U_{cw} being the wave and current velocity, f_{cw} the friction coefficient taking into account wave and current interaction and the subscript j should be replaced either by onshore or offshore.

Phase-lag effects in the sheet flow layer were included through the coefficient a_{pl} (Camenen and Larson, 2007) with:

$$a_{pl} = a_{onshore} - a_{offshore} \tag{16}$$

$$a_j = \frac{v^{0.25} U_{wj}^{0.5}}{w_s T_j^{0.75}} exp\left[-\left(\frac{U_{w,crsf}}{U_{wj}} \right)^2 \right] \tag{17}$$

where v is the kinematic viscosity of water, $U_{w,crsf}$ the critical velocity for the inception of sheet flow, U_w is the wave orbital velocity amplitude, W_s the sediment fall speed and the subscript j should be replaced either by onshore or offshore.

The suspended sediment load (q_{ss}) may be obtained from (Camenen and Larson 2007):

$$q_{ss,w} = U_{cw,net} \frac{c_R \varepsilon}{W_s} [1 - \exp\left(-\frac{w_s}{\varepsilon}\right)] \tag{18}$$

$$q_{ss,n} = U_c sin\varphi \frac{c_R \varepsilon}{W_s} [1 - \exp\left(-\frac{w_s}{\varepsilon}\right)] \tag{19}$$

where c_R is the reference concentration at the bottom, ε the sediment diffusivity, and $U_{cw,net}$, the net mean current.

The bed reference concentration is written as follows based on the analysis of a large data set on sediment concentration profiles (Camenen and Larson, 2007):

$$c_R = 3.51^{-3} \exp(-0.3 d_*) \, \theta_{cw,m} \exp\left(-4.5 \frac{\theta_{cr}}{\theta_{cw}}\right) \tag{20}$$

where d_* is the dimensionless grain size :

$$d_* = \sqrt[3]{(s-1) g / v^2} d_{50} \tag{21}$$

The sediment diffusivity was related to the energy dissipation from wave breaking according to Karambas and Koutitas (2002). Phase-lag effect in the suspended concentration due to ripples, is also incorporated according to Camenen and Larson (2007).
The nearshore morphological changes are calculated by solving the conservation of sediment transport equation (Leont'yev, 1996):

$$\frac{\partial z_b}{\partial t} = -\frac{\partial}{\partial x}\left(q_x - 2|q_x| \frac{\partial z_b}{\partial x} \right) - \frac{\partial}{\partial y}\left(q_y - 2|q_y| \frac{\partial z_b}{\partial y} \right) \tag{22}$$

where z_b is the local bottom elevation and $q_x (=q_{s,x}+q_{b,x})$, q_y $(=q_{s,y}+q_{b,y})$ are the volumetric sediment transport rates in x and y horizontal directions respectively.

4. Validating the hydrodynamic model

4.1. *Geometry of the model – Mesh generation*

The geometry which is implemented for the hydrodynamic model appraisal is based on the wave flume where the experiments of Ting and Kirby (1994, 1995, 1996) were conducted. There is a 40m long, 0.6m wide and 1m deep wave tank. A plywood false bottom was installed in the wave tank to create a uniform slope of 1:35. The still water depth in the constant-depth region of the wave tank was 0.4m in both the

experiments. The 2-D numerical model geometry is depicted below (Figure 1). There are 8 gauges for the spilling breaker, one offshore and 7 on the slope and 7 gauges for the plunging breaker, all of them placed on the slope. The start of the x and z axis is at the tow of the slope, as depicted in Figure 1.

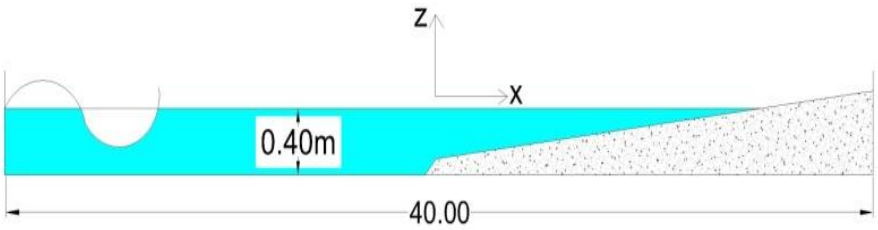

Figure 1. Sketch of the model's geometry

The mesh was generated with standard OpenFOAM tools, specifically with blockMesh and snappyHexMesh tools. First of all, the basic structured mesh with same-sized computational cells was created with blockMesh and then snappyHexMesh created the impermeable slope refining the appropriate cells. The refinement process has been done with snappyHexMesh as described in the OpenFoam tutorial and have been studied in some works (Gisen, 2014). The discretisation used is Δx=2cm and Δz=1cm. Appropriate boundary conditions were implemented.

4.2. *Numerical experiments – comparison with experimental data*

There are two cases that have been investigated in a previous work of the authors (Karagiannis et al., 2016), one for the spilling and one for the plunging breaker and compared satisfactorily with experimental data (Ting & Kirby, 1994, 1995, 1996). The results of the spilling breaker are presented briefly below.

4.2.1. *Spilling breaker*

The spilling breaker, is created for wave height H=0.125m and wave period T=2.0s and 8 gauged have been put on the slope.

Results for surface elevation, wave height and trough, wave setup, undertow and turbulent kinetic energy are presented below and compared satisfactorily with experimental data.

Figure 2 shows the distributions of wave height, trough and wave setup/setdown for both numerical and experimental results. The mean water level $\bar{\zeta}$ is measured from the still water level, whereas the maximum and minimum surface elevations are measured from the mean water level. It can be observed that numerical results are very close to experimental ones, especially for the wave setup/setdown and the wave trough. It must be noticed that the wave of the numerical model breaks earlier and it also cannot reach the maximum height of the wave of the experiment.

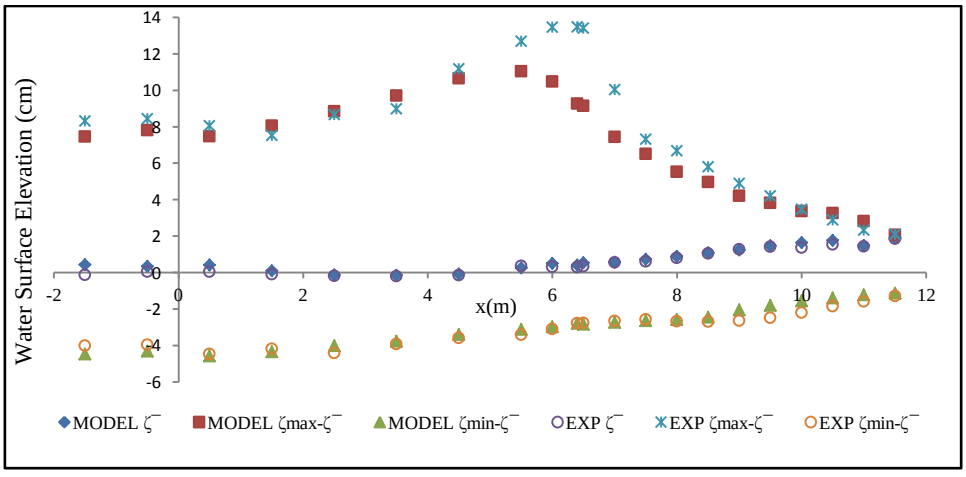

Figure 2. Distribution of wave height, trough and setup/setdown

Figure 3 shows the phase average water surface elevation for both numerical model and experiment at two different positions. The left one is referred to the position x=4.5m from the tow of the slope where the wave breaking has not occurred yet and the numerical surface elevation almost coincides with the experimental one. The right one is referred to the position x=8m after the wave breaking point and it can be observed that there is a little difference between the numerical and experimental surface elevation due to the earlier numerical wave breaking.

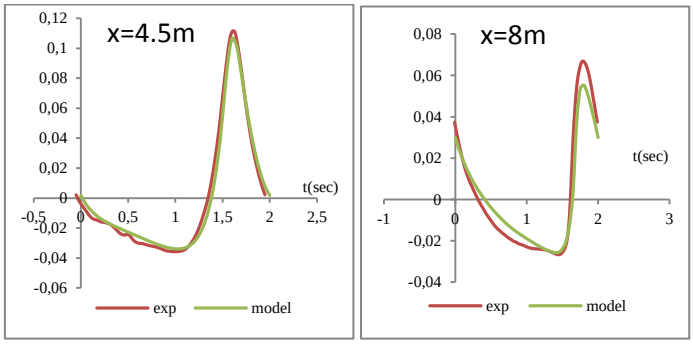

Figure 3. Phase average surface elevation before and after wave breaking

Figure 4 shows the instantaneous surface elevation for both numerical model and experiment at the same two positions with these in Fig.3. It can be observed that there is a difference between numerical and experimental results after the wave breaking, as expected.

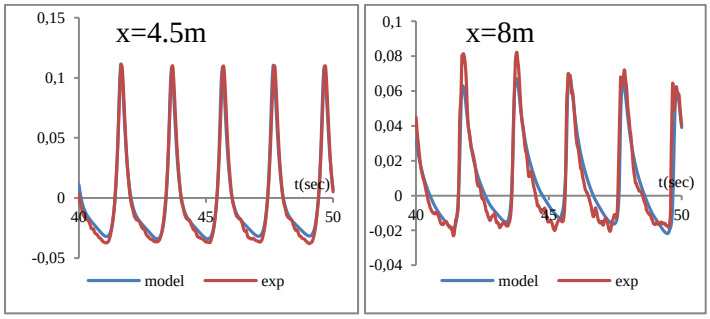

Figure 4. Instantaneous surface elevation before and after wave breaking

Numerical results for the undertow have been obtained and compared with experimental ones, as can be seen from the Fig.5. It is about the variation of time-mean horizontal velocity with depth and specifically the variation of the non-dimensional term($\bar{u}$ / gh) with depth that is depicted in Fig.5. The results are referred to the last 2 gauges placed on the slope after the wave breaking point. It can be noticed that the model behaves quite satisfactorily in terms of the undertow investigation at both gauges after the wave breaking point.

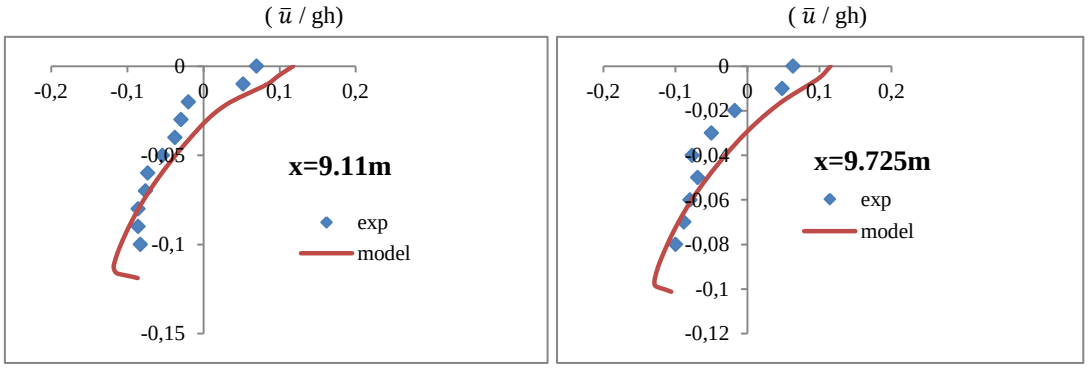

Figure 5. Variation of time-mean horizontal velocity with depth (undertow)

It can be observed from the Fig.5 that the model yields better undertow results as the gauge is closer to the shore after the wave breaking point.

The time-mean turbulent kinetic energy in the surf zone is presented in Fig.6. Specifically the non-dimensional term $(\bar{k} / gh)^{1/2}$ is plotted with depth for two gauges placed on the slope after the wave breaking point. It can be derived from Fig.6 that the model's results are close to the experimental ones.

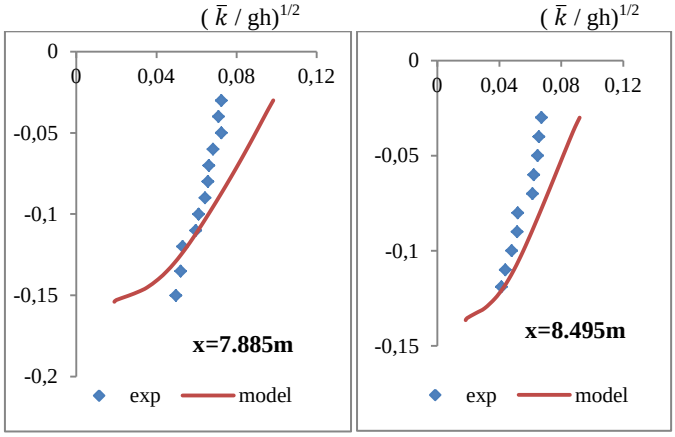

Figure 6. Variation of time-mean horizontal velocity with depth (undertow)

4.2.2. *Summary*

The surface elevation and wave height results seem to be quite satisfactory in comparison with experimental data although the wave breaking occurs a little bit earlier and the model does not reach exactly the highest surface elevation before breaking. From turbulence kinetic energy and undertow results can be concluded that the model somehow overestimates a little bit the turbulence before the breaking point, so early breaking occurs and higher turbulent kinetic energy and undertow numerical values are observed before the breaking point. Further calibration of the model may enhance the hydrodynamic results. However, the results are encouraging and it can be concluded that OpenFOAM is capable of simulating satisfactorily the wave propagation on beach slopes and the numerical results can be further used for sediment transport prediction.

5. Sediment transport – Numerical experiments

5.1. *Geometry of the model – Mesh Generation*

The geometry which is implemented for the numerical simulation of sediment transport is based on the wave flume where the SAFE (Dette et al.,1998) experiments were conducted. There is a 324m long, 5m wide and 7m deep wave tank. The beach was formed from a sand with d_{50}=300μm and a fall velocity of w_f=0.042m/s. The underwater profile from 4m above the flume floor was shaped to the equilibrium profile $h=0.12x^{2/3}$ where h is the water depth and x the distance from shore. The beach above the still water level (4m above the flume floor) has a slope of 1:20 for A1, A2 and A3 cases and 1:10 for the B2 case in the present work. The case of storm surges was investigated with random waves in the B2 case, so the water level was raised to 5m above the flume floor.

The mesh was generated with standard OpenFOAM tools, specifically with blockMesh and snappyHexMesh tools. First of all, the basic structured mesh with same-sized computational cells was created with blockMesh and then snappyHexMesh created the impermeable slope refining the appropriate cells. The refinement process has been done with snappyHexMesh as described in the OpenFoam tutorial and have been studied in some works (Gisen D., 2014). The discretisation used is Δx=0.5m and Δz=1cm. Appropriate boundary conditions were implemented.

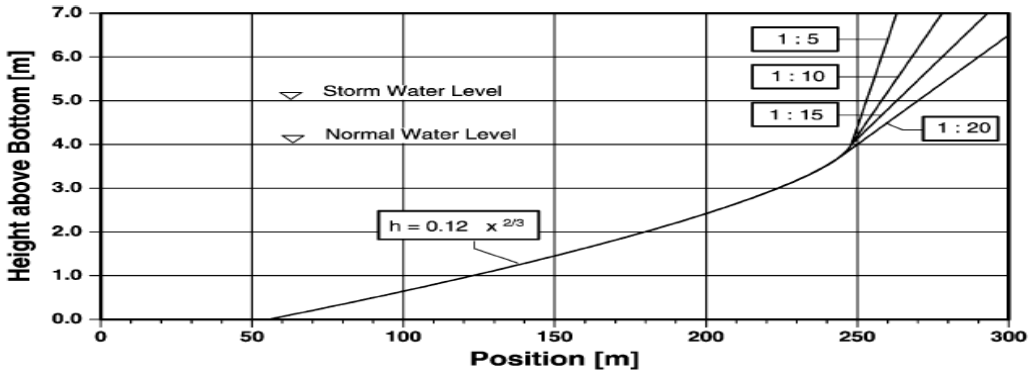

Figure 7. Sketch of the model's geometry (Dette et al., 1998)

5.2. *Numerical results*

It has been already mentioned that we numerically investigated and compared to experimental data 3 cases (A1, A2, A3) with 1:20 slope and we implemented the same monochromatic waves with those in the experiment (Dette, 1998). Also we implemented irregular waves to the slope of 1:10 according to B2 experiment (Dette, 1998).

The OpenFOAM model describes the wave propagation and the hydrodynamic characteristics of the flow are the input for the 2nd morphodynamic model which yields the seabed profile evolution. It has been mentioned that the method is repetitive, so the OpenFOAM model is implemented, then the hydrodynamic results are the input for the second morphodynamic model and the new seabed is arisen from the this model. Then, the new seabed is the input for the OpenFOAM model which is implemented again and yields new hydrodynamic results which are the input for the next implementation of the morphodynamic model which yields the new seabed and so on. The above process is repeated until convergence, namely the new seabed is practically the same with the previous one.

5.2.1. *A1 experiment (Dette, 1998)*

A monochromatic wave of height H=0.5m and period T=0.5s is implemented on the initial slope of 1:20. The seabed profile starts changing after the 1st run in the surf zone where erosion and a small bar are depicted in the left graph of Figure 8. The final profile seems to match satisfactorily the experimental data in the right graph of Figure 8 where a small bar and a notable erosion are formed in the surf zone and a small accretion in the swash zone.

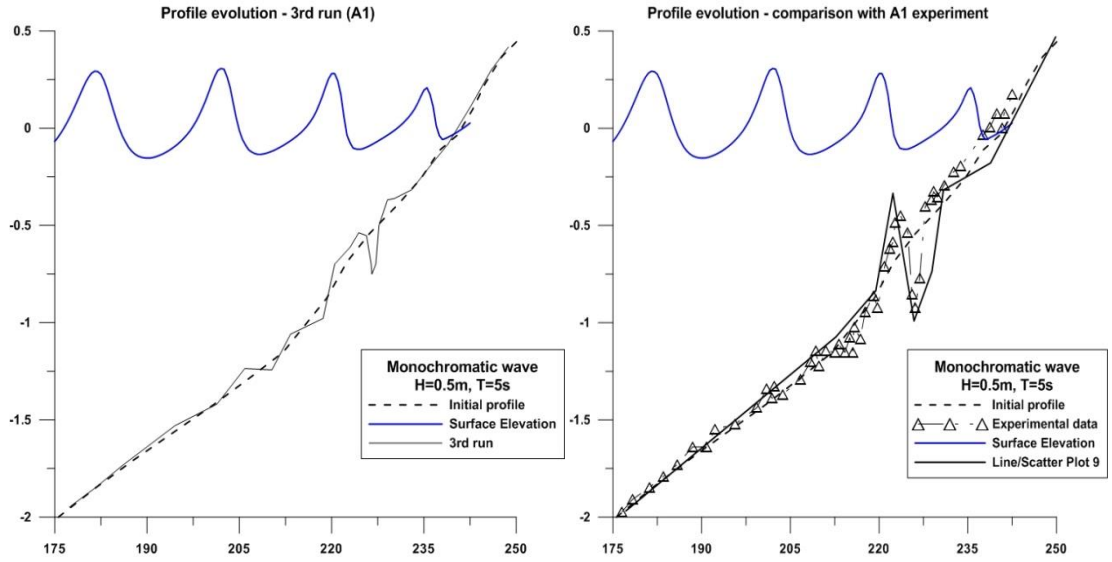

Figure 8. Profile evolution after the 3rd run and the final profile in comparison with A1 experimental data (Dette, 1998)

5.2.2. *A2 experiment (Dette, 1998)*
A monochromatic wave of height H=0.75m and period T=0.5s is implemented on the seabed as it was formed in the A1 experiment, namely the final formed seabed of the A1 experiment is the initial seabed for A2 experiment. The bar is shifting seawards firstly as it can be seen in the left graph of Figure 9 which refers to the 5th run while the erosion has disappeared in its previous intense form and some small changes occur onshore. The final seabed is formed after 12 runs with 3 bars and erosion areas respectively and small fluctuations seawards. It is compared satisfactorily to the experimental data as it can be observed in the right graph of Figure 9.

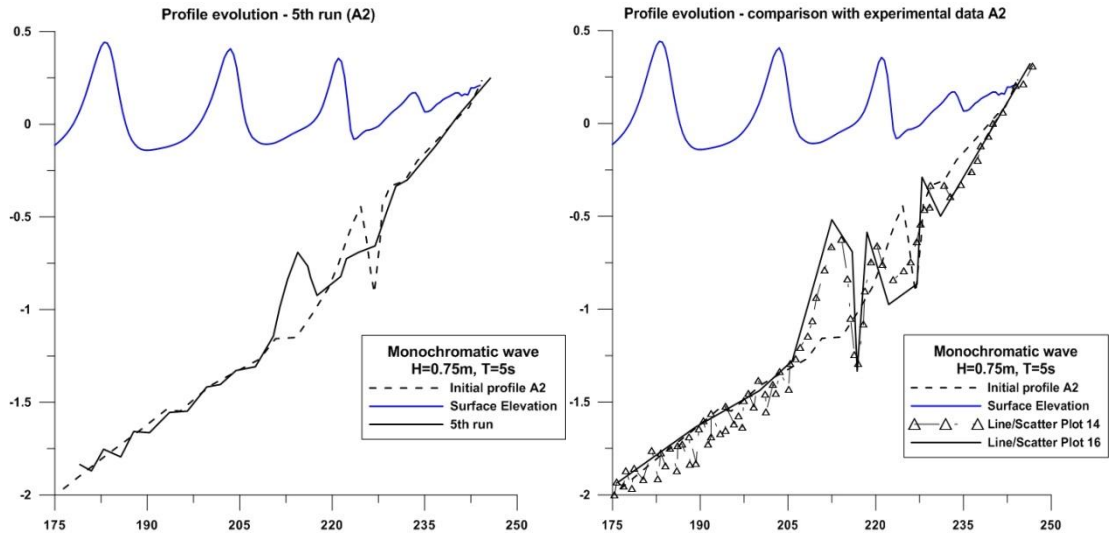

Figure 9. Profile evolution after the 5th run and the final profile in comparison with A2 experimental data (Dette, 1998)

5.2.3. *A3 experiment (Dette, 1998)*
A monochromatic wave of height H=1m and period T=0.5s is implemented on the seabed as it was formed in the A2 experiment. As described previously in A2 case, the final seabed as formed in the previous experiment is the initial seabed for this case. The bar is moving more seawards under the new hydrodynamic state and one bar exists in the surf zone while small changes occur in the swash zone where it seems that the new wave conditions do not affect so much the formation of the seabed in relation to the previous case. The numerical results are compared satisfactorily to the experimental data as it can be observed in the right graph of Figure 10.

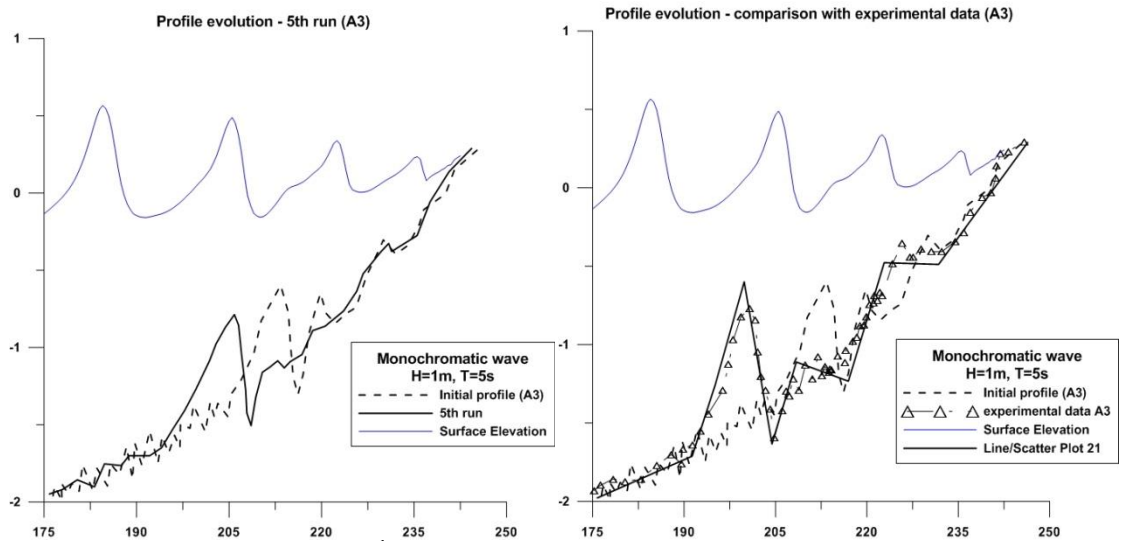

Figure 10. Profile evolution after the 5th run and the final profile in comparison with A3 experimental data (Dette, 1998)

5.2.4. *B2 experiment (Dette, 1998)*
A wave spectrum was applied with H_{m0}=1.20m and T_m=5.5s as the wave characteristics of the SAFE B2 experiment with 1:10 slope. Ten runs were needed until the seabed profile acquires its latest form and comparing this with the final profile from Test B2 experiment, it can be concluded that the numerical results fit the experimental ones quite satisfactorily. Figure 11&12 show 3 graphs of the profile evolution and its final form in comparison with experimental data respectively.

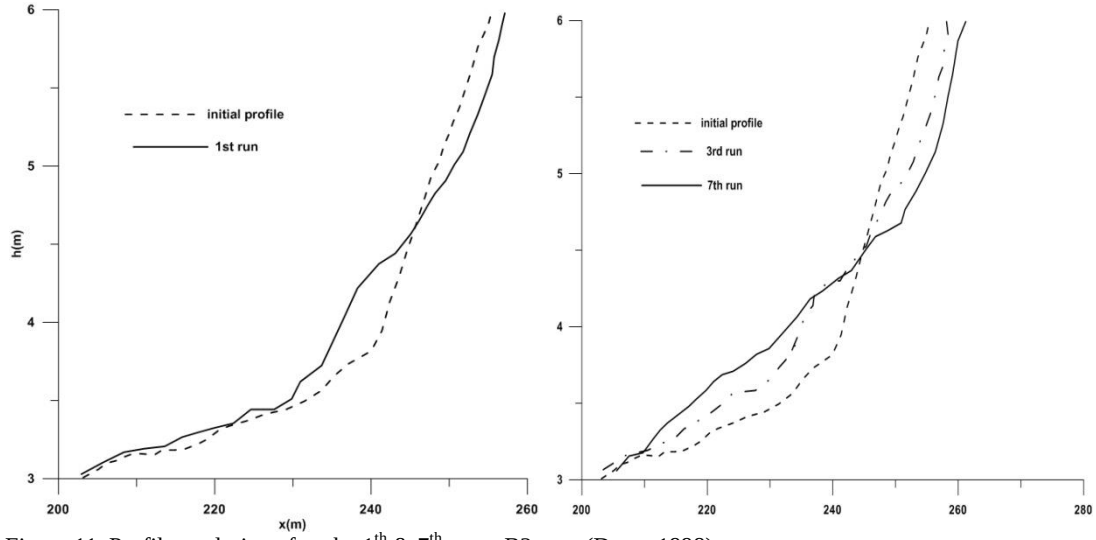

Figure 11. Profile evolution after the 1th & 7th run – B2 case (Dette, 1998)

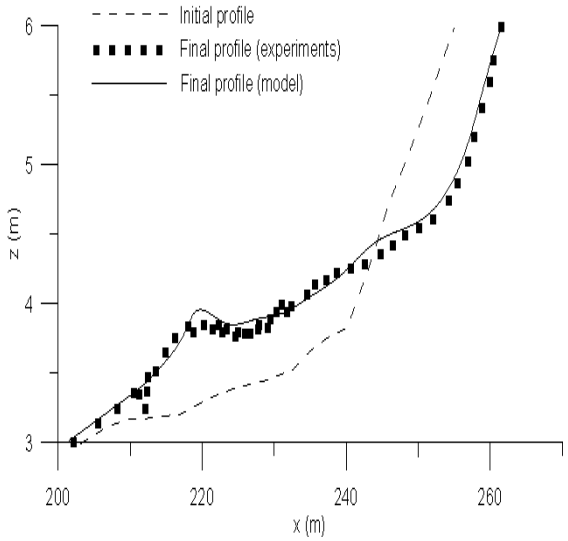

Figure 12. Final profile - comparison with experimental data B2 case (Dette, 1998)

6. Conclusions

- A challenging approach regarding the sediment transport modeling has been presented in this work where two numerical models have been developed, implemented and tested against experimental data. The method used here is repetitive using these two models alternately, one based on OpenFOAM platform producing the hydrodynamic state of each case and the other written in FORTRAN yielding the new seabed using the hydrodynamic results of the 1st one.
- The hydrodynamic model was first implemented and tested satisfactorily against experimental data (Ting & Kirby, 1994,1995,1996) comparing surface elevation, undertow and turbulent kinetic

energy results to the respective experimental ones.

- It seems that the OpenFOAM model overestimates the turbulent effects before the wave breaking, so the numerical wave breaks a bit earlier in comparison to the experimental one. Further calibration of the model will enhance the results.
- Three cases with monochromatic waves with 1:20 slope and one with irregular wave and 1:10 slope were investigated and tested against experimental data combining the two models.
- The combination of these two models is considered a holistic approach to sediment transport problems and it seems that it behaves quite well although it gives higher bars for A2 and A3 cases where the initial bed is the final one of the previous step where there are bars already formed.
- It seems that the bar is shifting seawards as the wave becomes higher but there are not so many changes in the swash zone.
- The surf zone is more affected by any new hydrodynamic state, especially with higher waves but the respond of the swash zone remains quite the same.
- A bar is formed in the surf zone under irregular waves while erosion is observed in the swash zone.
- The numerical results are compared satisfactorily to the experimental data but this method must be validated against more experiments with different wave conditions and steep slopes.

References

Camenen, B. & Larson. M. 2007. A unified sediment transport formulation for coastal inlet application, *Technical report ERDC/CHL CR-07-1, US Army Engineer Research and Development Center*. Vicksburg, MS.

Dette H.H., Peters K. and Newe J. 1998. ″ Large wave flume experiment ’96/97.″ *MAST III – SAFE Project*, Report No. 825.

Gisen D. 2014. “Generation of a 3-D Mesh Using SnappyHexMesh Featuring Anisotropic Refinement and Near-Wall Layers” *ICHE 2014*, Hamburg, Germany

Hirt C.W. & Nichols B.D. 1981. “Volume of fluid (VOF) method for the dynamics of free boundaries”, *Journal of Computational Physics*, 39 (1), 201-225.

Jacobsen, N.G., Fuhrman, D.R., and Fredsøe, J. 2012. ″A Wave Generation Toolbox for the Open-Source CFD Library: OpenFoam″. *Int. J. Numerl. Meth. Fluids,70*(9): 1073–1088.

Karagiannis N., Karambas T., Koutitas C. 2016. “Numerical simulation of wave propagation in surf and swash zones using OpenFoam”, *Proc ISOPE 2016,* June 26 – July 2, 2016, Rhodes, Greece

Karagiannis N., Karambas T., Koutitas C. 2016. “Numerical simulation of scour in front of a breakwater using OpenFoam”, *Proc 4th IAHR Europe Congress,* 27 - 29 July, 2016, Liege, Belgium, 309-315

Karambas Th. 2006. ″Prediction of sediment transport in the swash zone by using a nonlinear wave model″, *Continental Shelf Research*, 26, pp. 599-609.

Karambas Th. 2012. ″Design of detached breakwaters for coastal protection: development and application of an advanced numerical model″. *Proceedings of the 33rd International Conference on Coastal Engineering 2012*, 1(33), sediment.115. doi:10.9753/icce.v33.sediment.115

Karambas T. & Koutitas C., 2002. “Surf and swash zone morphology evolution induced by nonlinear waves”, *Journal of Waterway, Port, Coastal and Ocean Engineering*, American Society of Civil Engineers (ASCE), Vol. 128, no 3, pp. 102-113.

Menter, F.R. 1993. “Zonal Two Equation k-ω Turbulence Models for Aerodynamic Flows”, *AIAA Paper,* 93-2906.

Menter, F.R. 1994. “Two-Equation Eddy-Viscosity Turbulence Models for Engineering Applications”, *AIAA Journal*, vol. 32, no 8. pp. 1598-1605.

Ting, F. C. K. and Kirby, J. T. 1994. ″Observation of undertow and turbulence in a laboratory surf zone″. *Coastal Engineering* 24, 51-80.

Ting, F. C. K. and Kirby, J. T. 1995. ″Dynamics of surf-zone turbulence in a strong plunging breaker″. *Coastal Engine ering* 24 , 177-204.

Ting, F. C. K. and Kirby, J. T. 1996. ″Dynamics of surf-zone turbulence in a spilling breaker″. *Coastal Engineering* 27, 131-160.